Agricultural and Forest Meteorology xxx (2017) xxx–xxx

Contents lists available at ScienceDirect

Agricultural and Forest Meteorology

journal homepage: www.elsevier.com/locate/agrformet

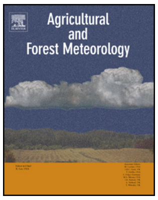

# Numerical study of the interplay between thermo-topographic slope flow and synoptic flow on canopy transport processes

Xiyan Xu[a,b], Chuixiang Yi[a,b,*], Leonardo Montagnani[c,d], Eric Kutter[a,b]

[a] *Queens College, City University of New York, Flushing, NY 11367, USA*
[b] *The Graduate Center, City University of New York, New York, NY 10016, USA*
[c] *Forest Services of Autonomous Province of Bolzano, via Bolzano 6, 39100, Italy*
[d] *Faculty of Science and Technology, Free University of Bolzano, Piazza Università 5, 39100, Bolzano, Italy*

ARTICLE INFO

*Article history:*
Received 17 September 2016
Received in revised form 7 February 2017
Accepted 8 March 2017
Available online xxx

*Keywords:*
Canopy flow
$CO_2$ transport
Complex terrain
Computational fluid dynamics
Recirculation
Synoptic winds
Slope wind

ABSTRACT

Canopy flow resulting from interaction between thermo-topographic slope flow and large-scale synoptic flow is very complicated and has been poorly understood. We apply a Reynolds-averaged Navier-Stokes (RANS) turbulence model to investigate how the interactions between local flow and synoptic winds affect $CO_2$ movement in the canopy layer at the Renon site in the Italian Alps. Since the RANS simulations are compared to the data measured by multiple-tower experiments conducted during CarboEurope-IP advection campaigns (ADVEX) at Renon, our study can be viewed as a case study of a relatively common wooded slope. The thermal condition in the canopy is directly related to the canopy morphology: the dense canopy at our site causes stronger cooling but limits vertical exchange of heat flux, resulting in weak temperature inversion in the deep canopy. Under conditions with no synoptic wind, local flow leads to $CO_2$ build-up mainly at downslope locations and no recirculation is formed. Recirculation that holds high $CO_2$ mole fraction in the canopy is developed only under the condition that local slope wind is enhanced by northerly synoptic winds. No recirculation forms when southerly synoptic wind direction is opposite to the local wind direction, in which case $CO_2$ is quite well mixed. This numerical study approach brings to light a better understanding of the $CO_2$ closure problem: the measured net ecosystem exchange of $CO_2$ is more likely to be underestimated in local non-synoptic slope flow and local synoptic-enhanced slope flow regimes at Renon. However, small-scale heterogeneity in canopy structure, variability in the $CO_2$ source from soil and higher-resolution and larger-scale topography still challenge the application of this numerical approach in the FLUXNET community.

## 1. Introduction

Accurate quantification of net ecosystem-atmosphere exchanges of mass and energy is a fundamental and critical step in reducing the uncertainty of how the large-scale climate change interacts with local ecosystems. The eddy covariance (EC) technique has proven to be a useful approach to quantify net ecosystem carbon exchange in the daytime when strong turbulent mixing occurs. In the night, nocturnal flux measurements ignore advection fluxes that can be of the same order as the eddy flux itself when flux sites are located in complex terrain (Massman and Lee, 2002; Feigenwinter et al., 2004, 2008, 2010a, 2010b; Aubinet et al., 2003; Aubinet, 2008; Aubinet et al., 2010; Aubinet and Feigenwinter, 2010; Finnigan, 2008; Goulden et al., 2006; Montagnani et al., 2009; Yi et al., 2000). The three-dimensional (3D) details of air movement, $CO_2$ transport, and temperature variation around the instrumented tower cannot be fully ascertained using EC measurements at a point, particularly in complex terrain. Massman and Lee (2002) stated that understanding of 2D and 3D flows and their role in micrometeorological flux observation is of great importance to any site; however, the problem of 2D and 3D flows is most difficult to evaluate at sites on non-flat terrain.

The errors of single tower measurements are more serious during calm nights in forested complex terrain, which is subject to the mechanisms of nocturnal canopy flow, *e.g.* turbulent ramps, gravity waves, intermittent turbulence, land, sea or lake breezes and drainage flows (Aubinet, 2008). The canopy flow resulting from interactions of site-specific topography and vegetation causes significant complexity in $CO_2$ transport that varies from case to case. At night periods, the ecosystem behaves as a $CO_2$ source because soil and above ground vegetation respiration are not offset by photosynthesis. $CO_2$ tends to accumulate near the ground due to surface

---

[*] Corresponding author at: School of Earth and Environmental Sciences Queens College, City University of New York, 65-30 Kissena Blvd, Flushing, New York 11367, USA.
*E-mail address:* cyi@qc.cuny.edu (C. Yi).

http://dx.doi.org/10.1016/j.agrformet.2017.03.004
0168-1923/© 2017 Elsevier B.V. All rights reserved.

layer stratification particularly in conditions of a super-stable layer within the canopy (Yi et al., 2005), resulting in strong negative vertical $CO_2$ gradients (Yi et al., 2008; Araújo et al., 2008). The negative vertical gradient of $CO_2$ with subsiding background wind contributes to positive vertical advection of $CO_2$ transport. Along the slope, much higher $CO_2$ concentration is commonly observed at lower altitude (slope and valley) than at higher altitude (plateau) (Araújo et al., 2008). The positive $CO_2$ gradient from high altitude to low altitude, along with drainage flow, results in a positive contribution to horizontal advection. Although positive advection in both vertical and horizontal is very common at night in sloped terrain, some observations reveal the complexity of the advection processes. For instance, airflow with low $CO_2$ concentration entrains from the top of the canopy to the surface contributing to a negative horizontal $CO_2$ gradient along the drainage flow direction and resulting in negative horizontal advection (Aubinet et al., 2003; Aubinet, 2008). Local terrain and vegetation effects can cause positive vertical velocity at night, resulting in negative vertical advection (Turnipseed et al., 2003). The vertical gradient of $CO_2$ distribution was found to be large on the upper slope but quite uniform on the lower slope (Reiners and Anderson, 1968; Araújo et al., 2008; Aubinet, 2008), implying smaller vertical advection in the $CO_2$-pooled valley than on the upper slope. All these observations have demonstrated the complexity and 3D effects of the advection on eddy flux measurements.

The eddy flux communities have made great efforts to conduct experiments with multiple-tower and multiple-level measurement systems to capture the 3D characteristics of wind fields and $CO_2$ movement to study the advection issues, such as the CarboEurope-IP advection campaigns (ADVEX) (Feigenwinter et al., 2008), advection measurements conducted at the AmeriFlux Niwot Ridge site (Sun et al., 2007; Yi et al., 2008) and tropical Amazon Rainforest (Tóta et al., 2012; Santana et al., 2017). The measured advection fluxes are of similar magnitudes as the turbulent fluxes during calm nights, and vary from site to site (Feigenwinter et al., 2008; Yi et al., 2008). The important feature is that the advection contribution is closely correlated to local and synoptic meteorological conditions. Local orographic flow is most likely to occur within the canopy, while synoptic wind is dominant above the canopy. However, synoptic flows can penetrate into the open canopy and interact with orographic flow (Sun et al., 2007). The process of interaction includes synoptic winds that enhance, attenuate, or even alter the direction of the orographic wind, depending on the direction and strength of prevailing synoptic winds (Feigenwinter et al., 2010a). Accordingly, the modified orographic flows have direct influence on $CO_2$ pooling or mixing, and hence on measured $CO_2$ flux.

Although the direct advection measurements provide insights into the wind fields and $CO_2$ transport at the research sites, the conclusions drawn may not be applicable to other FLUXNET sites subject to the conditions of local terrain and vegetation and large-scale synoptic conditions. In addition, the representativeness of the multiple-tower measurements is very sensitive to the tower setup and methodology used to derive the fluxes from measurements (Aubinet et al., 2010; Aubinet and Feigenwinter, 2010; Montagnani et al., 2010; Vickers and Mahrt, 2006). How can we take advantage of the single tower measurements found at most FLUXNET sites to understand 'site-specific' $CO_2$ transport processes? In this study, we aim to numerically resolve the 3D spatial variability of airflow and $CO_2$ transport initialized by measurements on one tower, but tested by multiple-tower experiments conducted during the ADVEX campaign at the Renon (RE) site in the Italian Alps. The airflows are simulated under various synoptic conditions to explore the interactions between local orographic flow and synoptic-scale winds, and related $CO_2$ processes. We hypothesize that (1) the interactive wind as a result of the synoptic and local slope winds varies with synoptic-scale weather patterns, (2) recirculation forms when synoptic and local winds enhance each other, and (3) canopy density along with the interactive winds leads to uneven heat and $CO_2$ transport: the cool air and $CO_2$ tend to pool in the recirculation zone and leeward slope (Fig. A1). We first describe the characteristics of terrain, vegetation and measurement set-up in Section 2, then we present the numerical method in Section 3 followed by results and discussions in Section 4. The conclusions are drawn in Section 5.

## 2. Site and data description

This numerical study is conducted based on the extensive measurements performed during the ADVEX campaign at the Renon-Selva Verde study site (RE, 46°25′ N, 11°17′ E,). RE is situated at about 1735 m above sea level in the Italian Alps, 12200 m North-Northeast of Bolzano. The Digital Elevation Model (DEM) of the 2000 m × 2000 m area around the RE is shown in Fig. 1 (labeled as D1). The topography of the site is characterized by alpine conditions with a main slope of about 11° that is locally oriented towards southeast in a mountain range having a principal North-South sloping direction. The vegetation at the site is characterized by a coniferous forest with gaps between groups of older and younger trees. The forest species are dominated by *Picea. abies* (85%), *Pinus cembra* (12%) and *Larix decidua* (3%), with a mean leaf area index (LAI) of 5.1 and maximal canopy height of 29–30 m in the 240 × 240 m research area (D2 in Fig. 1). The vegetation structure varies across the towers. A field survey in October 2009 classified the vegetation in D2 into three categories (Fig. 2): (1) Sparse forest in grassland, (2) Forest edge dominated by re-growth forest with sparse older trees, and (3) Mature forest.

The meteorological conditions at RE are dominated by the 'Tramontana' winds from the north or northwest (northerlies), typically in winter and occasionally in summer. Winds from the south (southerlies) tend to appear whenever there is a low-pressure system located over the Western Mediterranean area. Upslope (anabatic) winds during the day and down-slope (katabatic) winds during the night characterize the local (orographic) slope wind system.

An extensive measurement dataset (half-hourly averaged) was collected from the ADVEX campaign during May 1st to September 15th 2005. The ADVEX setup consisted of four external towers (A–D) and a permanent central tower (M) (Fig. A2). Each external tower was equipped for measurements of $CO_2$, $H_2O$, temperature, and wind vectors at heights of 1.5, 6, 12, and 30 m above ground level. An additional wind velocity measurement was made at 41.5 m on tower C. Measurement levels at tower M were 1.5, 6, 12, and 32m. A more detailed description of the site, measurement methods, and data processing can be found in Feigenwinter et al. (2008) and Montagnani et al. (2009).

## 3. Method

### 3.1. Conservation of mass and momentum

In configuring the numerical model, the flow is assumed to be steady state and the Boussinesq approximation is applied. The Navier-Stokes momentum and mass balance equations are applied to the canopy sub-layer with thermal stratification (Yi et al., 2005), which can be written as:

$$\frac{\partial \bar{u}_i}{\partial x_i} = 0, \tag{1}$$

$$\bar{u}_j \frac{\partial \bar{u}_i}{\partial x_j} = -\frac{1}{\rho}\frac{\partial P_*}{\partial x_i} + \nu \frac{\partial^2 \bar{u}_i}{\partial x_j \partial x_j} - \frac{\partial}{\partial x_j}\left(\overline{u_i' u_j'}\right) - g_i \beta \left(\bar{\theta} - \theta_\infty\right) - F_{Di}, \tag{2}$$

Please cite this article in press as: Xu, X., et al., Numerical study of the interplay between thermo-topographic slope flow and synoptic flow on canopy transport processes. Agric. Forest Meteorol. (2017), http://dx.doi.org/10.1016/j.agrformet.2017.03.004

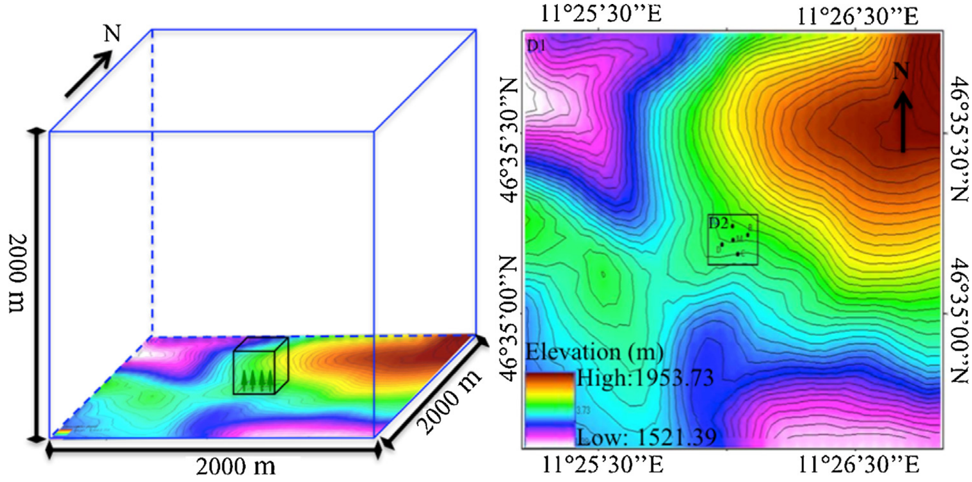

**Fig. 1.** The modeling domain and topography around Renon site. The five tower locations in the ADVEX campaign are indicated in the right panel. D1 is the outer domain (2000 × 2000 m) and D2 is inner domain (240 × 240 m) in our numerical simulation. The contour lines represent the elevations in the domain. The contour interval is 10 m.

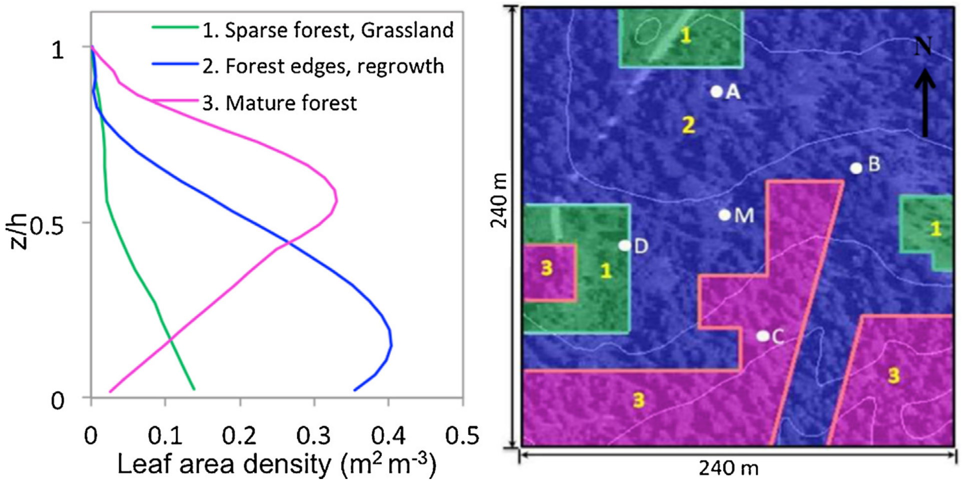

**Fig. 2.** Vertical leaf area density profiles of three vegetation categories (left panel) and their distribution in the 240 × 240 m research area (right panel) at Renon site: (1) Sparse forest in grassland, (2) Forest edge, and (3) Mature forest. The y-axis in left panel is normalized by each vegetation categories' canopy height ($h_1 = 21$ m, $h_2 = 24$ m, and $h_3 = 30$ m).

$$\bar{u}_j \frac{\partial \bar{\theta}}{\partial x_j} = \Gamma \frac{\partial^2 \bar{\theta}}{\partial x_j \partial x_j} - \frac{\partial}{\partial x_j}\left(\overline{\theta' u_j'}\right) + \frac{1}{\rho c_p} Q_{source}, \quad (3)$$

where $\bar{u}_i$ and $\bar{u}_j$ are the mean velocity components along the $x_i$ and $x_j$ directions, respectively, $\bar{\theta}$ is the mean potential temperature, $u_i'$, $u_j'$ and $\theta'$ are the fluctuations from their mean value $\bar{u}_i$, $\bar{u}_j$ and $\bar{\theta}$, ρ is the air density, $\nu$ is the kinematic viscosity of air, $P_*$ is the deviation of pressure from its reference value, and $\beta$ is the thermal expansion coefficient of air, $\theta_\infty$ is the reference temperature, $g_i$ is the gravity acceleration in $i$ direction, and $\Gamma = \nu/P_r$ is the turbulent viscous diffusion coefficient. Turbulent Prandtl number $P_r = 0.5$ is used for the canopy layer while in the region above the canopy (except very near the top of the canopy), $P_r = 1$ is used as applied in Xu et al. (2015). Following from Xu and Yi (2013), we have the following equation to define the drag force ($F_{Di}$) exerted by the canopy elements, which is zero above the canopy. In the canopy, $F_{Di}$ is calculated as:

$$F_{Di} = \frac{1}{2} K_r u_i |U|, \quad (4)$$

where $U$ is the horizontal scalar wind speed; and $K_r$ is the resistance coefficient (Wilson, 1986), which is derived from an empirical relationship originating from Hoerner (1965):

$$K_r = \frac{1}{2}\left[\frac{3}{2\phi} - 1\right]^2, \quad (5)$$

Where $\phi$ is the porosity of the canopy layer, which can be obtained from leaf area density $a(z)$ (Gross, 1993):

$$\phi(z) = \frac{\sqrt{1 + 4a(z)} - 1}{2a(z)}, \quad (6)$$

The energy source $Q_{source}$ is specified as upward radiative heat flux.

### 3.2. *Conservation of scalar quantities*

The conservation for scalar $CO_2$ with mean molar mixing ratio ($c$) is given by:

$$\bar{u}_j \frac{\partial \bar{c}}{\partial x_j} = D \frac{\partial^2 \bar{c}}{\partial x_j \partial x_j} - \frac{\partial}{\partial x_j}\left(\overline{c' u_j'}\right) + S_c, \quad (7)$$

where $\bar{u}_j$ is solved by Eqs. (1) and (2), $c'$ is the fluctuation from its mean value $\bar{c}$, $D$ is the molecular diffusivity of $CO_2$. The $CO_2$ source term $S_c$ from the ecosystem is associated with belowground respiration ($R_b$) from soil and aboveground respiration ($R_a$) from plant leaves, stems and roots.

Please cite this article in press as: Xu, X., et al., Numerical study of the interplay between thermo-topographic slope flow and synoptic flow on canopy transport processes. Agric. Forest Meteorol. (2017), http://dx.doi.org/10.1016/j.agrformet.2017.03.004

### 3.3. $CO_2$ source parameterization

$CO_2$ source term $S_c$ is parameterized with total ecosystem respiration (TER) of belowground respiration ($R_b$) and aboveground respiration ($R_a$), where $R_a = \sigma \cdot R_b$. Here $\sigma$ is a proportionality coefficient fulfilling $TER = R_b + R_a$. The net contribution of $CO_2$ from the belowground respiration is quantified as the Q10 exponential relation with soil temperature (Van t'Hoff, 1884). Although the soil respiration was demonstrated to have significant spatial variability at the Renon site (Acosta et al., 2013) we neglect here its spatial variability. For simplicity, the empirical formula (Montagnani et al., 2009) obtained at RE is used to quantify

$$R_b = R_{ref} Q_{10}^{\left(T - T_{ref}\right)/a}, \tag{8}$$

where $R_{ref} = 3.69\,\mathrm{mol\,m^{-2}\,s^{-1}}$ is the respiration rate at reference temperate $T_{ref} = 10°\,\mathrm{C}$, $Q_{10} = 3.64$ is the factor by which $R_b$ increases for an increase in soil temperature of $a = 10\,°\mathrm{C}$.

Foliage respiration is usually assumed to be exponentially related to air temperature (Law et al., 2001; Ohkubo et al., 2007; Urban et al., 2007). However, based on relatively small vertical temperature differences (~2–3 °C) measured at the same time from a single tower at the RE site, we assume that foliage respiration depends on the leaf area density and its temperature dependence is negligible. Since soil respiration accounts for about 63% of forest ecosystem respiration as suggested by Janssens et al. (2001), total respiration above ground is $R_a = (37/63) \cdot R_b$. We partition the above ground respiration to multi-layers using the leaf area distribution similar to the CANVEG model (Baldocchi and Meyers, 1998). For each vertical layer $k$ at the height $z_k$, above ground respiration is:

$$R_a\left(z_k\right) = R_a \left\{ \frac{1}{LAI} \sum_{z=k-1/2}^{k+1/2} a\left(z\right) \right\}. \tag{9}$$

### 3.4. Turbulence model

We used the Renormalization Group (RNG) $k$–$\varepsilon$ model developed by Yakhot and Orszag (1986). RNG techniques are used for the large scale motions in which the effects of the small scales are represented by modified transport coefficients. The RNG $k$–$\varepsilon$ turbulent model has been successfully applied in reproducing topographic and canopy related flows under different atmospheric stability conditions (Kim and Patel, 2000; Xu and Yi, 2013; Xu et al., 2015).

The Reynolds stress in Eq. (2), turbulent heat flux in Eq. (3) and turbulent $CO_2$ flux in Eq. (7) are linked to turbulent viscosities of momentum ($\mu_t$, heat $\left(\mu_\theta = \mu_t / P_r\right)$ and $CO_2$ ($\mu_c = \mu_t / S_c$)), respectively, as

$$-\overline{u_i' u_j'} = \mu_t \left( \frac{\partial \bar{u}_i}{\partial x_j} + \frac{\partial \bar{u}_j}{\partial x_i} \right) - \frac{2}{3} \delta_{ij} k, \tag{10}$$

$$-\overline{\theta' u_j'} = \mu_\theta \frac{\partial \bar{\theta}}{\partial x_j}, \tag{11}$$

$$-\overline{c' u_j'} = \mu_c \frac{\partial \bar{c}}{\partial x_j}, \tag{12}$$

$\delta_{ij}$ is Kronecker delta, and $k$ is the turbulent kinetic energy. Turbulent Prandtl number $P_r$ is the same as in Eq. (3), the turbulent Schmidt number $S_c$ is 0.6 as suggested by Flesch et al. (2002) and applied in Xu and Yi (2013). $\mu_t$ in Eq. (10) is calculated in terms of turbulent kinetic energy $k$ (TKE) and dissipation $\varepsilon$:

$$\mu_t = \rho C_\mu \frac{k^2}{\varepsilon}, \tag{13}$$

where $k$ and $\varepsilon$ are solved from the TKE transport equations; $C_\mu$ is a dimensionless constant.

In RNG $k$–$\varepsilon$ turbulent model, the steady-state transport equation of TKE and its dissipation are written as:

$$\bar{u}_i \frac{\partial k}{\partial x_i} = \frac{\partial}{\partial x_i} \left( \frac{\mu_t}{\sigma_k} \frac{\partial k}{\partial x_i} \right) + P_s + P_b + P_w + T_p - \varepsilon, \tag{14}$$

$$\bar{u}_i \frac{\partial \varepsilon}{\partial x_i} = \frac{\partial}{\partial x_i} \left( \frac{\mu_t}{\sigma_\varepsilon} \frac{\partial \varepsilon}{\partial x_i} \right) + C_{\varepsilon 1} \frac{\varepsilon}{k} P_s - \rho C_{\varepsilon 2} \frac{\varepsilon^2}{k} - S, \tag{15}$$

where $P_s$ is shear production, given by:

$$P_s = \mu_t \frac{\partial \bar{u}_i}{\partial x_j} \left( \frac{\partial \bar{u}_i}{\partial x_j} + \frac{\partial \bar{u}_j}{\partial x_i} \right), \tag{16}$$

$P_b$ is buoyancy production, given by:

$$P_b = -\mu_\theta g_i \beta \frac{\partial \bar{\theta}}{\partial x_i}, \tag{17}$$

$P_w$ is wake production. In vegetation canopy, $P_w$ is caused by the work of the canopy drag force and reads as:

$$P_w = \bar{u}_i F_{Di} = \frac{1}{2} K_r |U| \bar{u}_i^2, \tag{18}$$

$T_p$ is transport of TKE by pressure perturbation, which is calculated as a residual of other TKE components , $S$ is a volumetric source term, proposed by Yakhot et al. (1992):

$$S = \frac{C_\eta \eta^3 \left(1 - \frac{\eta}{\eta_0}\right) \varepsilon^2}{\left(1 + \beta_0 \eta^3\right) k}, \tag{19}$$

$$\eta = \frac{k}{\varepsilon} \left[ \frac{P_s}{\mu_t} \right]^{1/2}, \tag{20}$$

where the empirical constants $C_\mu$, $\sigma_k$, $\sigma_\varepsilon$, $C_{\varepsilon 1}$, $C_{\varepsilon 2}$, $\beta_0$, and $\eta_0$ are 0.0845, 0.7194, 0.7194, 1.42, 1.68, 0.012, and 4.38, respectively, These empirical constants are derived by the Renormalized Group procedures with scaling and approximation proposed by (Yakhot and Orszag, 1986), but refined by Yakhot and Smith (1992) and Yakhot et al. (1992) to fix the closure problems in the original derivations.

### 3.5. Numerical implementation

The main goal of this research is to understand the relationship among the three-dimensional wind field, temperature, and $CO_2$ level at Renon with heterogeneous vegetation, particularly under nocturnal stable atmospheric conditions. Three measurement time periods were identified to provide initial conditions for three cases: (1) 00:30 Local Standard Time (LST) of day 192–24:00 LST of day 193 characterized by synoptically driven *Northerlies*; (2) 00:30 LST of day 206–06:00 LST of day 207 characterized by *Southerlies*, when the sky was dominantly overcast; and (3) 12:00 LST of day 207–24:00 LST of day 211 characterized by a *local slope wind system*. For each case, the half-hourly average of each variable measured at the central tower M during nocturnal time window (21:00–04:00 LST) in relevant measurement time period above was used as initial condition and heat fluxes measured on the ground were used as boundary conditions.

The computational domain extends over 2000 m × 2000 m in the outer domain (D1), with a 240 m × 240 m inner domain (D2) located in the middle of the outer domain (Fig. 1) for the horizontal plane. In the vertical, D2 extends from the lowest surface in D2 to a height at which the vertical domain satisfies the height of at least three times the forest height in D2. D1 extends to 2000 m high from the lowest surface in the 2000 m × 2000 m domain. The domain is divided into multi-block to accommodate the varied elevation and grid spacing. In each block, Cartesian coordinates are applied with the finest

Please cite this article in press as: Xu, X., et al., Numerical study of the interplay between thermo-topographic slope flow and synoptic flow on canopy transport processes. Agric. Forest Meteorol. (2017), http://dx.doi.org/10.1016/j.agrformet.2017.03.004

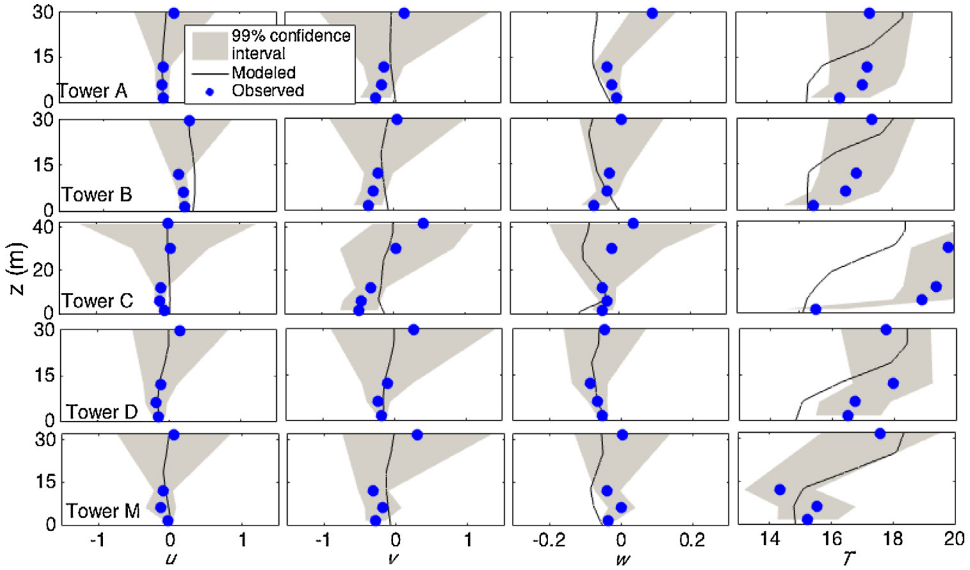

**Fig. 3.** The profiles of variables ($u$, ms$^{-1}$; $v$, ms$^{-1}$; $w$, ms$^{-1}$; $T$, °C) at 99% confidence level for **local slope wind** measured at A–D and M towers during the nighttime period (9:00 p.m.–4:00 a.m. LST) from ADVEX campaign (light blue), showing the lower and upper values of the variables at the measurement height. The blue dots indicate the average values over the nighttime period at the measurement height. The black solid lines denote the profiles by the numerical model. (For interpretation of the references to colour in this figure legend, the reader is referred to the web version of this article.)

**Table 1**
Typical wind systems and modeling periods.

| Cases | Time Period (LST) | |
|---|---|---|
| Northerlies | 00:00, July 11 (day 192) | 00:00, July 13 (day 194) |
| Southerlies | 00:00, July 25 (day 206) | 06:00, July 26 (day 207) |
| Slope wind | 00:00, July 28 (day 209) | 00:00, July 30 (day 211) |

grid spacing in D2. The schematic diagram of the mesh at the intersection of Tower M is shown in Fig. A3. The shaved cell method along with the cell-combining approach is applied to the cut cells at the air-ground interface (Yamazaki and Satomura, 2010). The local slope wind condition case is used to test the ideal model grid spacing by changing horizontal and vertical grid spacing between 1–10 m in D2 and accordingly stretched grid spacing in D1. The grid spacing that fits the calm night in local slope wind period should be capable of resolving air flows during nights with stronger northerlies and southerlies. Because of the weak wind and high variation in wind direction, we use the confidence interval of 99% to plot the lower and upper bounds of the measured variable $R$ (u, v, w, T) at the measurement heights. The ideal grid space setting for the three cases is based on the standard that about 70% of modeled variables are within 99% confidence interval of the measurements (Fig. 3). Meanwhile, two fully convergent criteria are required. One is that $(\gamma^{i+1}-\gamma^{i})/\gamma^{i} \leq 10^{-5}$, where $i$ is the iteration number and $\gamma$ is any of the dependent variable. Another is that the normalized residuals for momentum, energy, mass and turbulent variables are required to be lower than $10^{-3}$. The ideal horizontal grid space at D2 is 4 m and at D1 it is stretched with a power law, starting with a horizontal grid spacing of 4 m at the edge of the forest and about 11 m at the lateral boundaries. The ideal grid spacing in vertical is 3 m from ground surface to at least three times the canopy height (90 m) and similarly stretched using a power law, starting with 3 m at the top of three times the canopy height and extending to about 15 m at the top of D1 domain boundary. The stretching power in both horizontal and vertical is 1.3. With this grid setting, there are about 76% of the modeled variables within 95% confidence interval of the measurements for local slope wind period. The topography is extracted from the NASA Shuttle Radar Topographic Mission (SRTM) 90 m digital elevation data v4 (Jarvis et al., 2008). The SRTM elevation data is fitted to 4 × 4 m grids with Kriging interpolation. The distribution of three canopy classifications covering D2 is shown in Fig. 2. The outer region (D1) is covered by grassland to a larger extent than D2, where we treat it as bare land and specify the ground surface roughness height of 0.8 m for computational purposes.

The prescribed wind profile function is used for wind velocity at the north and south inflow boundaries of 2000 m × 2000 m domain for northerlies and southerlies, respectively,

$$U_B(z)=\frac{u_*}{k}ln\left(\frac{z+d}{z_0}\right) \tag{21}$$

where $d = 0.6h$ is the zero plane displacement height, $h$ is the height of canopy. $z_0 = 0.8$ m is roughness length. The friction velocity u* is derived by the relation that $-\overline{u'w'}=u_*^2$, where $-\overline{u'w'}$ is measured by the sonic anemometer at level 4 (32m) on the permanent Tower M, based on the assumption that Reynolds stress is constant above the canopy (Yi, 2008). The vertical velocity at the inflow boundary is specified to be zero. At the outflow boundaries, a zero gradient boundary condition is applied. The zero gradient boundary condition is specified for the top and four lateral boundaries of local slope winds (Table 1).

The ambient temperature is $\theta_0(z)=\theta_{00}+\gamma z$, where $\theta_{00}$ is the potential temperature at z = 0, which is specified with soil temperature measured at the depth of 5 cm, $\gamma$ is ambient lapse rate, set to $-6^{\circ}$ C km$^{-1}$ that is the approximate lapse rate for a summer night in the Italian Alps (Rolland, 2002). The energy source ($Q_{source}$) at the top of the canopy is taken from the measured sensible heat at 32 m. We assume that within the canopy $Q_{source}$ is an exponential function of downward accumulative leaf area density $L(z)=\sum_{z'=z}^{h}a(z')$,

$$Q(z)=ae^{-\mu L(z)}+b, \tag{22}$$

where $\mu$ is the canopy extinction coefficient. Our sensitivity analysis indicates that the profile of Q(z) in Eq. (22) is insensitive to $\mu$, which is in the range (0.4, 0.65) of the conifer canopies (Pierce and Running, 1988). 0.52 is used for $\mu$ in this simulation. $a$ and $b$ are constants (Table A1) determined by heat flux $Q_h$ at the top of the canopy and ground heat flux $Q_g$ at z = 0. The values of $Q_h$ and $Q_g$ used for three different synoptic conditions are shown in Table 2.

Please cite this article in press as: Xu, X., et al., Numerical study of the interplay between thermo-topographic slope flow and synoptic flow on canopy transport processes. Agric. Forest Meteorol. (2017), http://dx.doi.org/10.1016/j.agrformet.2017.03.004

**Table 2**
Parameter values used in the model set-up.

| Cases | $Q_h$ (Wm$^{-3}$) | $Q_g$ (Wm$^{-2}$) | $T_a$ (°C) | $T_{00}$ (°C) |
|---|---|---|---|---|
| Northerlies | −47.49 | −0.39 | 9.81 | 9.04 |
| Southerlies | −2.47 | 1.26 | 12.54 | 12.37 |
| Slope wind | −10.53 | 1.81 | 15.94 | 14.44 |

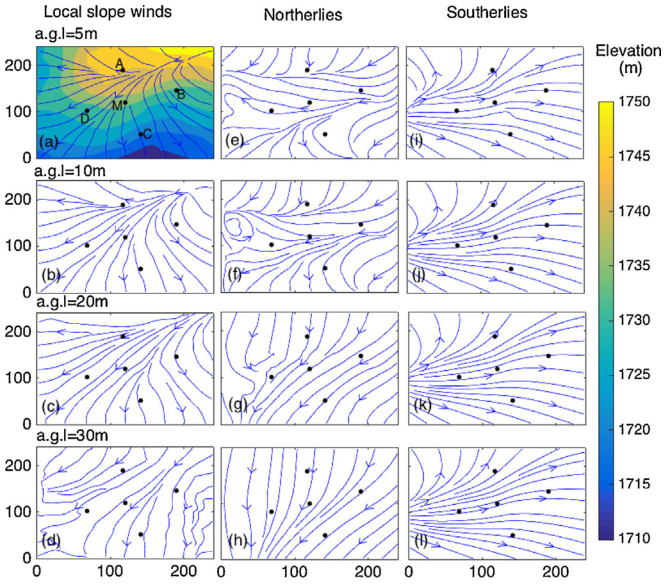

**Fig. 4.** Simulated wind streamlines at vertical levels above ground: *a.g.l.* = 5(1st row), 10(2ed row), 20 (3rd row) and 30 (4th row) m in 240 × 240 m domain for Local slope wind (left panel: a–d), Northerlies (middle panel: e–h) and Southerlies (right panel: i–l). The colored isolines in (a) denote the elevation in the 240 × 240 m domain. The solid dots denote the locations of Towers that are labeled in (a). The height of the canopy is 24 m at Tower A, B and M, 30 m at Tower C and 21 m at Tower D.

## 4. Results and discussions

### 4.1. Mean wind field

#### 4.1.1. Local slope winds

The local slope winds are a thermally forced drainage flow regime ($w < 0$) without synoptic scale disturbance (Figs. 3 and 4a–d). Winds generally blow towards the south-east along the diagonal of D2, following the direction of slope. However, in the north, easterly drainage winds are dominant due to the presence of a secondary slope falling to the east above about $y = 150$ m (Fig. 4a–d). In the south, winds shift from southwest to south because of the lowest elevation between $x = 100$ and 200 m where the slope is steepest (Fig. 4a–d). The drainage winds are only significant within the canopy, and the flow patterns remain similar at all levels through the canopy (Fig. 4a–d). However the streamlines become inflected at the top of the canopy. The inflection is caused by canopy disturbance, which is notable when drainage winds become very weak (Turnipseed et al., 2003). Above the canopy, air is sinking into the canopy (Fig. 5), i.e., only vertical velocity is important and the slope-following wind patterns are diminished due to reduced thermal-topographic effects.

The drainage flow is determined by the balance of hydrodynamic pressure gradient, hydrostatic pressure gradient (buoyancy force) and drag force, while the turbulence stress can be ignored after the turbulence collapses under stable conditions (Sedlák et al., 2010). Under stable conditions, the Froude number derived from dimensional analysis of hydrodynamic and hydrostatic pressure gradient is much smaller than 1 (Belcher et al., 2012), suggesting the dominant thermal-topographic effects of buoyancy force, which is given as:

$$F_{hs} = g\left(\frac{\Delta\theta}{\theta_0}\right)\sin\alpha, \tag{23}$$

where α is the slope angle, $\Delta\theta$ is the potential temperature difference between the ambient air and the colder thermo-topographic slope flow, and $\theta_0$ is the ambient potential temperature (Chen and Yi, 2012). Fig. 5 shows that the wind profiles at Towers A, B and M display similar profile shape with a maximum wind speed around 0.15–0.20 ms$^{-1}$. The maximum wind at Tower A is much smaller than that at Towers B and M, because buoyancy forces are small at Tower A where the slope is gentler than at Tower B and M. On a gentle slope, the drainage flow is enhanced with the steepness of slope and the canopy effects are stronger (Chen and Yi, 2012). Towers A, B and M are surrounded by re-growth forest that is characterized by dense foliage in the lower canopy. The dense foliage exerts a large drag force on the drainage flow near the ground surface. The level of maximum wind speed is therefore elevated up to about mid-canopy, while most drainage flow occurs at lower trunk-level in open-trunk forests (Turnipseed et al., 2003; Yi et al., 2005; Belcher et al., 2008).

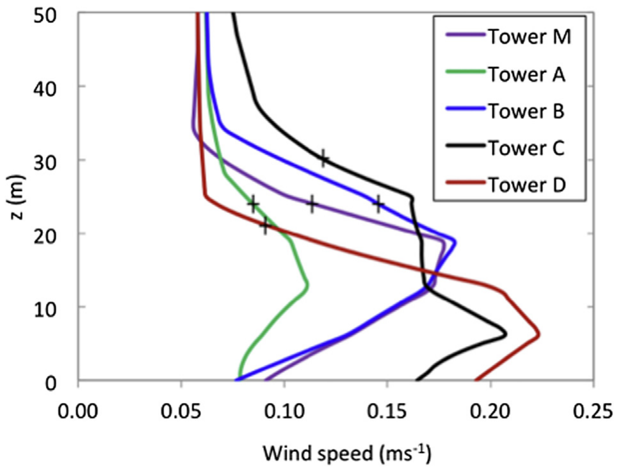

**Fig. 5.** Simulated wind profiles at five towers during local slope wind periods. The black crosses denote the top of the canopy at each tower.

The mature forest as observed at the site and in our model configuration is characterized by typical foliage distribution with open trunk space and maximum leaf area density in the upper canopy. Wind profile at Tower C is determined by the canopy morphology of mature forest with a primary wind maximum at the trunk region and a secondary wind maximum near the top of the canopy. Although drag force at Tower C is significant, wind speed at Tower C remains strong compared with wind speed at Towers on the upper slope. This is because the hydrostatic buoyancy force is large enough to maintain drainage flow on the steep lower slope. In addition, airflow experiences long slope acceleration before reaching Tower C. Although Tower D experiences a small hydrostatic buoyancy force, it encounters the strongest drainage flow near the ground surface, which is caused by the smaller drag force due to sparse trees in the grassland. The fast attenuation of wind speed from ground surface to the top of the canopy at Tower D indicates that thermal forcing is only important near the ground surface for the sparse canopy, because of the leaf area density related heat flux source.

#### 4.1.2. Northerlies

During northerlies periods, wind direction and wind speed of the local slope winds are modified after interacting with synop-

Please cite this article in press as: Xu, X., et al., Numerical study of the interplay between thermo-topographic slope flow and synoptic flow on canopy transport processes. Agric. Forest Meteorol. (2017), http://dx.doi.org/10.1016/j.agrformet.2017.03.004

tic northerlies (Fig. 4e–h). As the slope generally falls to the south with the effects of the valleys in the south-east and west, the wind is blowing towards the south or southwest direction at the boundary of the research domain, or else is diverted to the west in the northern part of the domain, where there's a slope falling to the west. These easterly drainage flow induced winds only occur in the lower canopy (Fig. 4e and f). Winds twist from the southwest to the south in the southern part of the domain, where the elevation is lowest and the slope is steepest. The topographic effects decrease with height and become very weak at the top of the canopy (Fig. 4h), where northerlies prevail. Even so, we can still see southward winds in the southeast due to the steep slope. The initial prescribed wind speed of northerlies is about 7.4 $\mathrm{m\,s^{-1}}$ at the top of the canopy, according to Eq. (21). The strong northerlies enhance local slope winds both within and above canopy. The enhancement is much stronger in the upper canopy and above canopy than in deep canopy. The limited influences of northerlies on local slope winds within canopy demonstrate that deep canopy flow is governed by local radiative forcing of the topography and vegetation instead of downward momentum transport from synoptic northerlies above the canopy.

A remarkable flow pattern is the up-slope winds blowing to the northwest in the lower canopy between Towers M and A. This up-slope motion is associated with the recirculation region in the south-north (S-N) direction (Fig. 7a) and updraft in the west-east (W-E) direction (Fig. 7c). Instead of occurring on the lower level of the lee slope, the recirculation occurs at the gentle upper slope in our research domain, which is attributed to the vegetation structure and distribution. Our simulation (D1) is conducted for the bare land surrounding the forests. As the wind blows from the northern bare land into the forest, it lifts after passing the sparse trees in the grassland that is located north of Tower A. Between Towers A and M, the dominant vegetation is re-growth forest with sparse older trees characterized by the dense foliage at trunk level. The dense canopy exerts a large drag force, which retards flow in the deep canopy, resulting in a region of reversed flow, i.e. recirculation, underlying the lifted flow. A similar upward action was observed in stable nighttime conditions at the Niwot Ridge Ameriflux site, which is also partly explained by vegetation distribution (Turnipseed et al., 2003). The explanation of flow convergence within canopy is also applicable to our results. Flow from north and east converges between Towers A and M, forcing a rising motion.

The recirculation bubbles extend through the re-growth forest in the S-N direction (Fig. 7a and b). The reversed flow ends before reaching the edge between re-growth and mature forest in the west (cross sections at $x = 88$, 104, and 120 m in Fig. 7a and b). In the east, the extension of reversed flow is further north than that in the west. The reversed flow extends across the edge between re-growth and mature forest, because of northward extension of mature forest. At S-N cross section $x = 88$ m (Fig. 7a and b) where northerlies experience the far expansion of re-growth forest, the recirculation breaks into two at about $y = 136$ m. From the west to east, the average depth of the recirculation region (mean height at $v = 0$) increases from 8 m to about 10 m, which confirms that increasing slope angle leads to increasing depth of recirculation (Xu and Yi, 2013). The maximum depth of recirculation is at the mid-canopy, about 15–16 m high.

The updraft motion in the west domain is due to temperature difference in the W-E direction (Fig. 7c and d), which is mainly driven by vegetation distribution. In the east domain, re-growth forest and mature forest are dominant. LAI for both forests is around 5. The dense canopy radiates much more long-wave radiation than the grassland with LAI around 1, leading to stronger cooling in the east. As the colder air from the east advances into the less dense warmer air in the west, the lighter warm air is lifted upward. In front of the lifted flow, the region is characterized by reversed flow (eastward) above a shallow layer of westward wind near the ground surface.

#### 4.1.3. Southerlies

The modification of southerlies to local slope winds is significant, although the southerlies are relatively weak (Fig. 4i–l). Wind speed of local slope winds is strengthened but with altered wind direction. The predicted wind speed is weaker than 0.5 $\mathrm{m\,s^{-1}}$ at the top of the canopy, which is much weaker than prescribed southerlies (about 3 $\mathrm{m\,s^{-1}}$) but stronger than local slope winds. In the north, winds remain southerly with up-slope motion ($w > 0$ at Towers A and M). However, the westerlies occur ($u > 0$) in the south. This westerly component is much stronger than the southerly component, leading to cross-slope flow instead of up-slope flow (Fig. 4i). The altered flow pattern remains significant up to triple canopy height above which the southerlies become dominant.

Streamlines at the cross sections show the flow pattern in both the vertical and horizontal during southerly wind periods (Fig. 8). Air sinks above the canopy during southerly wind period, because southerlies are weak. In the S-N direction, air subsides strongly in the south between $y = 80$ and 100 m (Fig. 8a) where there is stronger radiative cooling from mature forest. The subsiding air diverges to the north and south near the ground surface. On the northern upper slope, the slope is gentle, so weak local slope winds are reversed by the prevailing southerlies. In the south, the steep slope results in strong drainage flow overwhelming the southerlies. Even so, the drainage flow is not strong enough to reverse southerlies but both flows interact to become westerly winds. The westerly winds are accompanied with sinking motion from above the canopy.

### 4.2. Thermal analysis

Temperature inversion develops in all the vegetation canopies due to radiative cooling. However, the temperature distribution and vertical profiles are different under different prevailing wind systems and vegetation categories.

#### 4.2.1. Local slope winds

During local slope wind periods, the significant temperature difference between in- and above canopy is caused by radiative cooling in the vegetation canopy (Fig. 6a and c). The cooling occurs all through the canopy, resulting in temperature differences of 3–3.5° C between ground surface and the canopy top. This temperature difference is in the range of observed temperature differences in the 10 m high walnut orchard (Dupont and Patton, 2012) and 21.5 m high aspen forest (Mahrt et al., 2000) under stable conditions with weak wind. The uneven distribution of the cooled air at the top of the canopy is caused by the leaf area density difference in the modeled three canopy shapes. Weak cool air pooling within canopy in the downwind direction is caused by cold air draining down the slope. A relatively warmer canopy layer at the domain boundaries is due to no canopy-depth cooling outside of the 240 × 240 m domain where no vegetation is in the model set-up.

Temperature profiles reveal that an inversion occurs in the upper canopy because of strong radiative cooling, above which temperature profiles become uniform with height for all the forest types because of no cooling source (Fig. 9a). The temperature profiles are different in the lower canopy, which is directly induced by the canopy structure-related radiative cooling. At Towers A, B and M, the dominant re-growth forest is characterized by dense foliage below about 12 m, above which temperature inversion is developed. The inversion becomes very weak below 11 m. At Towers M and B, negative temperature gradient is found below 6 m, resulting in a 'cold bulge' at about 6 m where leaf area density reaches its maximum. The maximum leaf area density in the lower canopy reduces the effects of radiative cooling above 6 m, so the thermal

Please cite this article in press as: Xu, X., et al., Numerical study of the interplay between thermo-topographic slope flow and synoptic flow on canopy transport processes. Agric. Forest Meteorol. (2017), http://dx.doi.org/10.1016/j.agrformet.2017.03.004

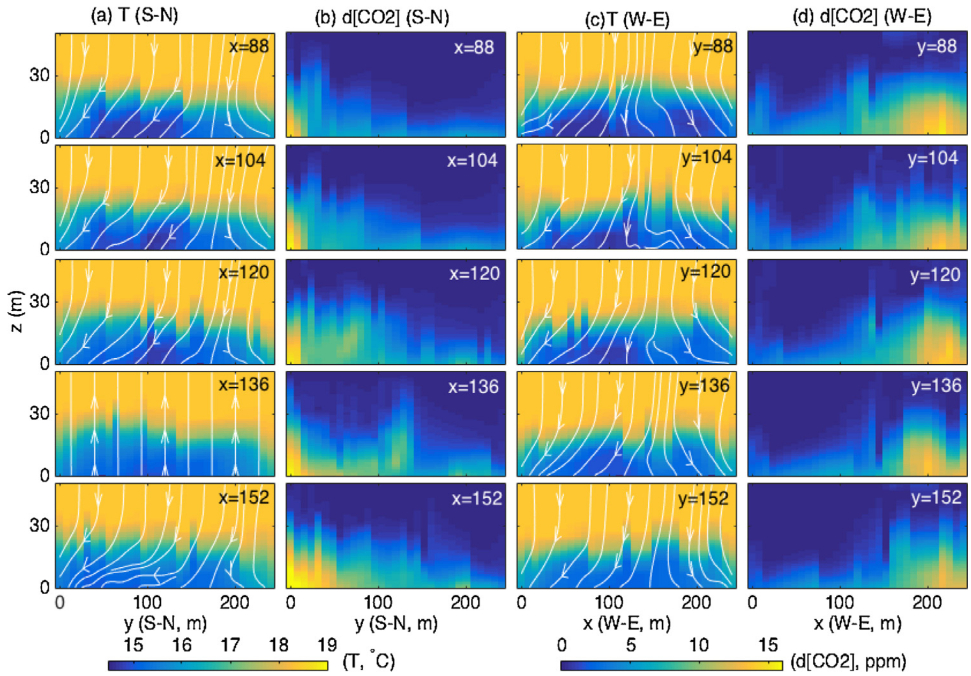

**Fig. 6.** Simulated distribution of Temperature (T, °C) and $CO_2$ difference (d[$CO_2$], ppm) at cross sections during **Local slope** wind periods in the S-N direction: (a) Temperature and (b) $CO_2$ difference; the W-E direction: (c) Temperature and (d) $CO_2$ difference. The white solid lines with arrows denote the wind streams at the cross sections.

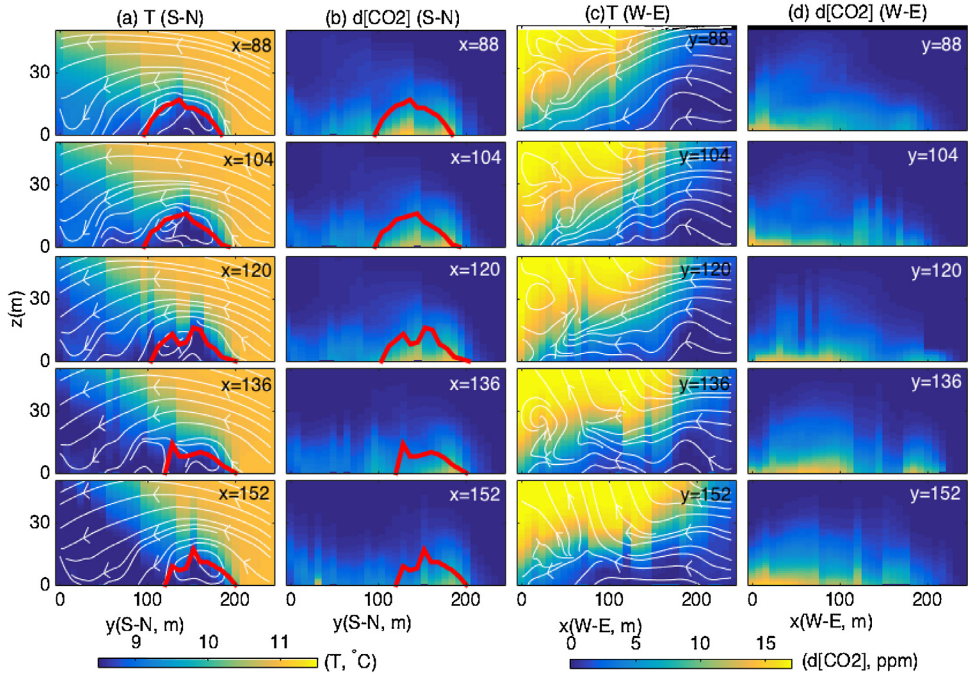

**Fig. 7.** Simulated distribution of Temperature (T, °C) and $CO_2$ difference (d$CO_2$], ppm) at cross sections during **Northerly** wind periods in the S-N direction: (a) Temperature and (b) $CO_2$ difference; the W-E direction: (c) Temperature and (d) $CO_2$ difference. The white solid lines with arrows denote the wind streams at the cross sections. The pink solid lines in (a) and (b) denote the top of reversed flow.

condition below 6 m is mainly determined by ground heat flux. The positive ground heat flux during local slope wind period leads to weaker inversion and warmer air near the ground surface, implying the near-neutral or even unstable layer in dense canopy (Shaw et al., 1988; Jacobs et al., 1994; Dupont and Patton, 2012; Xu et al., 2015). In the lower canopy, temperature at Tower M is about 0.5 °C colder than temperature at Towers A and B, because Tower M is at downwind direction of slope wind, experiencing cooled drainage flow. In the upper canopy, air at tower B is about 0.5 °C colder than at Towers A and M, because Tower B is located at about 10 m east to the mature forest (Fig. 9a). A stronger cooling in the upper dense canopy of mature forest can enhance cooling in the upper canopy of re-growth forest in the neighborhood.

Temperature profiles at Tower C depicts the cooling in the upper canopy of mature forest with the coolest air and strongest temperature inversion above the height of 17 m compared with temperature at other towers (Fig. 9a). In the lower canopy, the temperature inversion is reduced due to weak radiative cooling in

Please cite this article in press as: Xu, X., et al., Numerical study of the interplay between thermo-topographic slope flow and synoptic flow on canopy transport processes. Agric. Forest Meteorol. (2017), http://dx.doi.org/10.1016/j.agrformet.2017.03.004

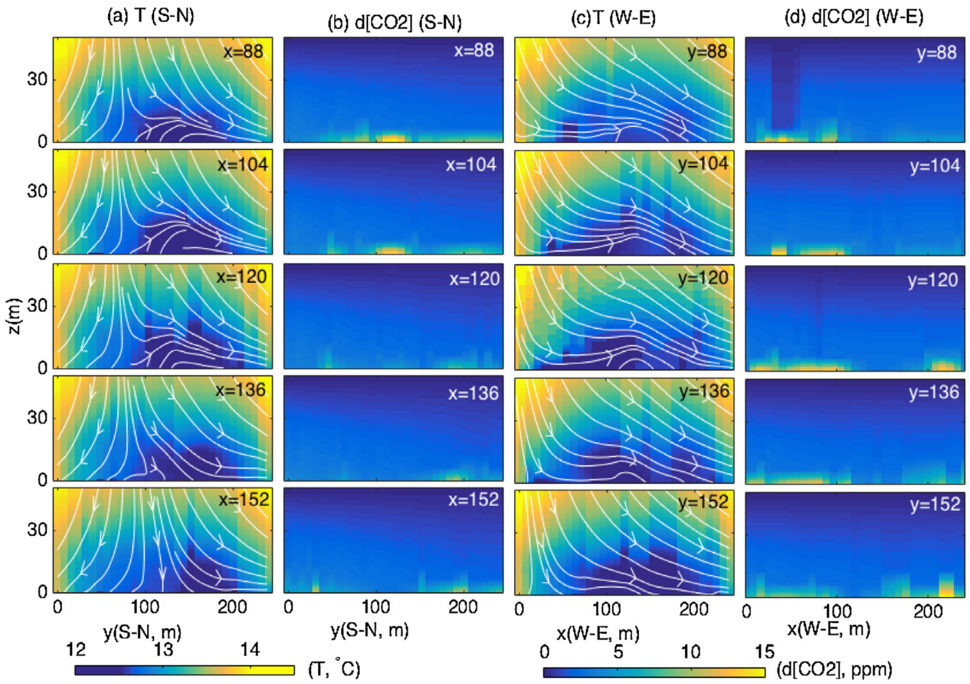

**Fig. 8.** Simulated distribution of Temperature (T, °C) and $CO_2$ difference ($dCO_2$], ppm) at cross sections during **Southerly** wind periods in the S-N direction: (a) Temperature and (b) $CO_2$ difference; the W-E direction: (c) Temperature and (d) $CO_2$ difference. The white solid lines with arrows denote the wind streams at the cross section. The black dashed lines in (a) and (b) denote the boundary where the winds diverge to south and north.

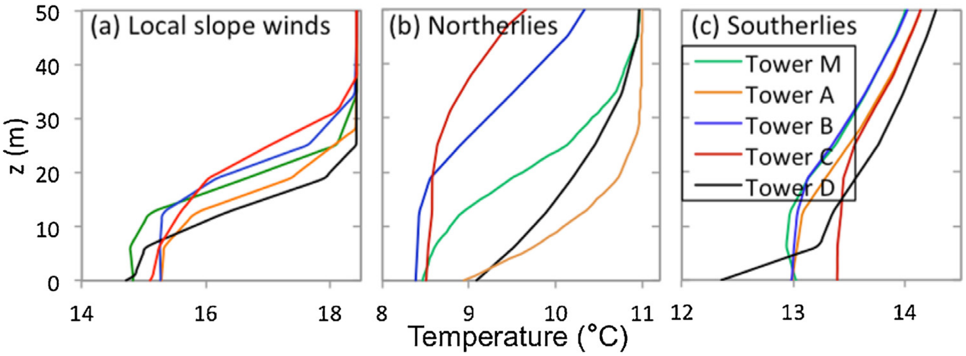

**Fig. 9.** Simulated temperature profiles at five towers during prevailing wind periods (a) Local slope winds, (b) Northerlies and (c) Southerlies.

the lower canopy and positive ground heat flux. In contrast, temperature inversion at Tower D is significant in the lower canopy with warmer temperature above 8 m due to the fact that Tower D is surrounded by sparse trees in grassland with its maximum leaf area density at ground surface. Radiative cooling in sparse trees in grassland is stronger in the lower canopy than at the same height in re-growth and mature forest. The strong cooling in the lower canopy overwhelms surface positive heat flux, which results in strong inversion near the ground surface.

#### 4.2.2. *Northerlies*

During northerly wind periods, air is warmer in the north but cooler in the region of recirculation and south (Fig. 7a). The warmer north is attributed to the higher elevation and gentler slope, when cold air drains to the lower elevation. Wind in the recirculation region is weak and reversed, resulting in cool air stagnation. In the south, the downslope northerlies drain cooler air to the lower slope, especially in the southeast, where elevation is lowest and slope is steepest in the domain. The temperature gradient in the W-E direction is mainly attributed to the vegetation distribution. Most of the mature forest is distributed in the east where stronger radiative cooling occurs, leading to relatively cooler east and warmer west. The temperature difference is responsible for the updraft flow in the W-E direction.

During northerly wind periods, the maximum temperature difference from the top of the canopy to the ground surface is about 2.5 °C (Fig. 9b). The temperature difference is much smaller and less variable compared with local slope wind periods, which can be explained by strong northerlies causing better mixing throughout the canopy. Temperatures at Towers A, B and M surrounded by re-growth forest are very similar to temperature during slope wind periods: warmest temperature is at Tower A, which is at more elevated upwind direction; coldest temperature is at Tower B, which is close to dense mature forest with strong radiative cooling; temperature at Tower M is intermediate between Towers A and B. The difference in profile shape is related to the flow pattern during northerly wind periods. Towers A and M are located in the region of recirculation. The temperature in the reversed flow is about 3 °C cooler than air in the upwind direction on the upper slope (Fig. 7a). Unlike temperature at Towers B and M, temperature inversion is very strong in the lower canopy at Tower A, because Tower A is located at the boundary of reversed flow, experiencing

Please cite this article in press as: Xu, X., et al., Numerical study of the interplay between thermo-topographic slope flow and synoptic flow on canopy transport processes. Agric. Forest Meteorol. (2017), http://dx.doi.org/10.1016/j.agrformet.2017.03.004

strong temperature gradient in both the horizontal and vertical. The temperature profile at Tower C shows coldest air in the upper canopy and weak inversion in the lower canopy as the profile during local slope wind periods. Temperature at Tower D indicates homogeneous cooling in grassland due to its canopy structure and strong wind mixing.

#### 4.2.3. Southerlies

During southerly wind periods, the temperature variation is lower than 2 °C in the research domain (Fig. 8), which is induced by both very weak cross-slope wind mixing and radiative cooling under the overcast sky conditions. The weak drainage flow cannot effectively drain the cold air down the slope. The temperature difference is less than 1 °C between ground surface and the top of the canopy at all the towers except Tower D (Fig. 9c). At Towers A–C and M, temperature inversion only develops in the upper to above canopies. Temperature is almost constant in the lower canopy (below 10 m high), due to less radiative cooling and the positive ground surface heat flux. Temperature at Tower A is still warmer than at Towers B and M, but with larger temperature difference throughout the canopy. The effects of mature forest cooling on temperature at Tower B becomes trivial, showing a minor difference in temperature above 20 m at Towers B and M. The 'cold bulge' occurring during local slope wind periods is also present during southerly wind periods at Tower M because of positive heat flux from the ground surface.

Although the cooling in the dense mature forest at Tower C is stronger than at other towers, temperature at Tower C is relatively warmer and inversion is weaker than at Towers A, B, and M, which is contrary to the condition during local slope wind and northerly wind periods. The warmer temperature at Tower C can be partially explained by the weak radiative cooling during southerly wind period. Although Tower C is located on the slope of the drainage flow, the drainage flow isn't strong enough to pool cool air in the lower slope. At Tower D, temperature is warmest in the upper canopy and inversion is strongest near the ground surface, as during local slope wind periods. The highest foliage density related radiative cooling in the lower canopy dominates the thermal condition near the ground surface.

### 4.3. $CO_2$ distribution

$CO_2$ emission rate is only determined by soil temperature in Eqs. (8) and (9). The total amount of $CO_2$ emission is very similar for different canopies experiencing the same wind period, because the temperature difference on the ground surface is very small. $CO_2$ emission rate is varied vertically at levels dependent on leaf area density distribution in Eq. (9). Here we use $CO_2$ mole fraction deviation (d[CO2]) from the mean atmospheric $CO_2$ mole fraction to analyze the $CO_2$ transport in the domain.

During local slope wind periods, $CO_2$ is built up in the south and east (Fig. 6b and d). In the S-N direction, a maximum of 17 ppm higher $CO_2$ level is in the downwind of the local slope wind as compared to the upper slope (Fig. 6b). Particularly high $CO_2$ accumulates in the southeast, where slope is steep and elevation is low. Relatively high level of $CO_2$ can extend north to the upper slope and fill in the whole canopy layer, which is related to the distribution of mature forest. In the W-E direction, $CO_2$ level is high in the east due to the westerly slope wind (Fig. 6d). We expect the $CO_2$ level in the west is as high as in the east because of the westward slope winds. However, it shows good mixing in the west, probably due to sparse trees in grassland in the west, which makes it easier for $CO_2$ to vent out of the canopy. Relatively stronger wind in the lower canopy and wind shear throughout the canopy at Tower D, as compared to Tower B, can be demonstrated by the wind profiles in Fig. 5.

During northerly wind periods, $CO_2$ is built up in the recirculation region in the S-N direction, which coincides with cool air pooling on the middle to upper slope (Fig. 7b and d). The highest $CO_2$ level is in the west where the recirculation occurs farther south owing to the reduced extent of mature forest there. Most of the $CO_2$ is restricted below about 16m, above which $CO_2$ is well mixed by strong prevailing northerlies. On the lower slope of the downwind direction, there is no obvious transport of $CO_2$ from elevated prevailing northerlies, as $CO_2$ is mainly emitted from the ground surface (Fig. 7b). In the W-E direction, elevated $CO_2$ is confined to a very shallow layer on the ground surface, mostly in the west, which is caused by flow descending from east to west (Fig. 7d). The updraft flow has minor influence on $CO_2$ transport because the updraft flow is at a higher elevation.

During southerly wind periods, much better mixing of $CO_2$ is seen in comparison with northerly and local slope wind periods, although there is a very shallow layer below 6 m with higher level of $CO_2$ (Fig. 8b and d). $CO_2$ distribution in the surface shallow layer is quite homogeneous along the slope. The $CO_2$ mole fraction deviation from the atmospheric $CO_2$ mole fraction is mostly smaller than 10 ppm due to the accompanied sinking motion with the cross-slope flow. The cross-slope winds enhance the $CO_2$ mixing in the canopy layer. Even on the upper slope, the $CO_2$ difference is about 6 ppm due to descending winds flowing northward.

### 4.4. Overview of model-measurement comparisons

As the prescribed boundary conditions are tested against the local slope wind, our model shows best prediction for local downslope drainage flow (Fig. 3). About 70% of the model predictions at the measurement heights are within 99% confidence interval of measurements. Among the five towers, the model underpredicts the measured mean wind speed. Haiden and Whiteman (2005) indicated that the drainage flow accelerates down the long slope. However, our modeling domain (D1) is just a small part of the long north-to-south slope, so that the acceleration on the upwind slope out of the modeling domain is missed.

During northerly wind periods, our model successfully predicts the down-slope wind measured at all the towers except at Tower A where the wind is blowing from north to south with upward motion (Fig. 10). The upward motion ($w$ is increasing with height) indicates flow convergence in the lower canopy. During southerly wind periods, our model predicts south winds flowing throughout the canopy (Fig. 11). However, just above and in the upper canopy, predicted southerlies are much weaker than the measured southerlies but stronger than pure local slope winds. This can reflect the interactions between southerlies and drainage flow. The predicted $u$ component is opposite to the measurements during both northerlies and southerlies because the westerly component in the synoptic northerlies and easterly component in synoptic southerlies (Feigenwinter et al., 2010a) have not been taken into account in our model. It implies that wind direction is very sensitive to the large-scale wind regime. However, the large-scale wind direction cannot be determined simply by the measurement near the top of the canopy, because of the canopy flow characteristics near the canopy top (strong shear, inflection, etc.).

It is encouraging that our model shows a better prediction in the deep canopy than in the upper canopy, when compared with tower measurements. It is due to airflow in deep canopy being dominated by local thermo-topographic forcing, while predictions in upper canopy are the result of interactions between local slope winds and synoptic winds. However, the representations of synoptic influences in our local-scale model are very limited. Our model predicts the typical nocturnal temperature profiles in the canopy: temperature inversion in the upper canopy due to outgoing longwave radiation and isothermal or inversion profile in the lower

Please cite this article in press as: Xu, X., et al., Numerical study of the interplay between thermo-topographic slope flow and synoptic flow on canopy transport processes. Agric. Forest Meteorol. (2017), http://dx.doi.org/10.1016/j.agrformet.2017.03.004

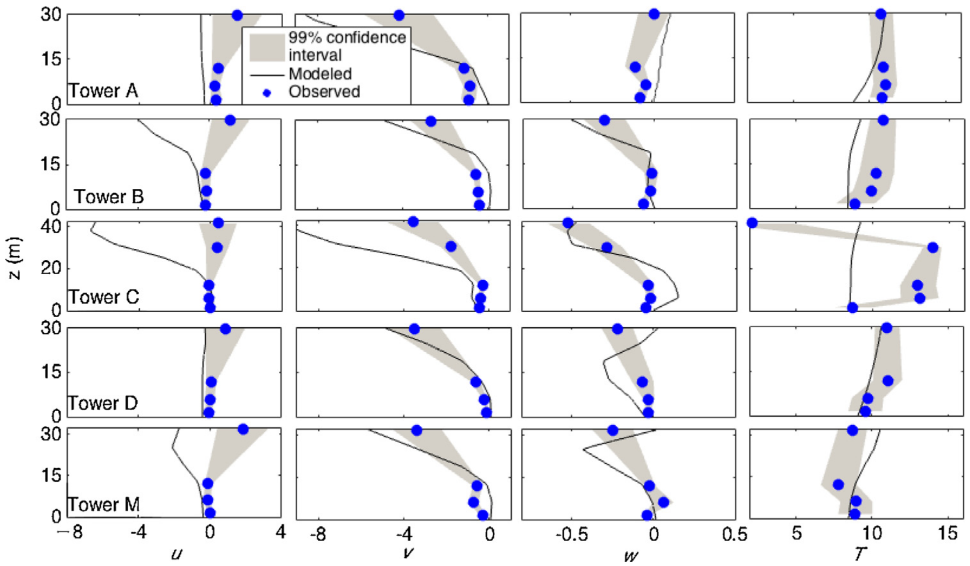

**Fig. 10.** The profiles of variables ($u$, ms$^{-1}$; $v$, ms$^{-1}$; $w$, ms$^{-1}$; $T$, °C) at 99% confidence interval for **northerly winds** measured at A–D and M towers during the nighttime periods (9:00 p.m.–4:00 a.m. LST) from ADVEX campaign (light blue), showing the lower and upper values of the variables at the measurement height. The blue dots indicate the average values over the nighttime period at the measurement height. The black solid lines denote the profiles by the numerical model. (For interpretation of the references to colour in this figure legend, the reader is referred to the web version of this article.)

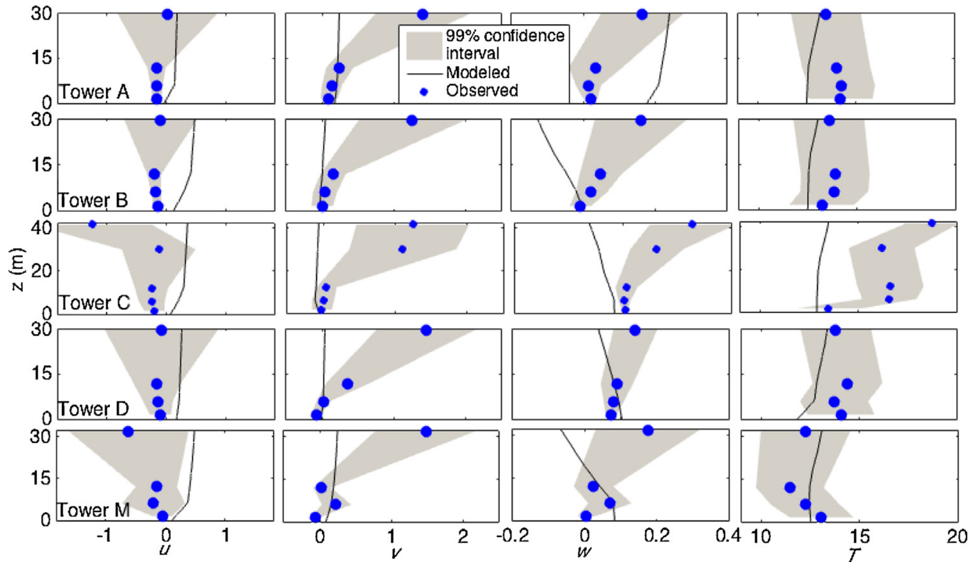

**Fig. 11.** The profiles of variables ($u$, ms$^{-1}$; $v$, ms$^{-1}$; $w$, ms$^{-1}$; $T$, °C) at 99% confidence interval for **southerly winds** measured at A–D and M towers during the nighttime period (9:00 p.m.–4:00 a.m. LST) from ADVEX campaign (light blue), showing the lower and upper values of the variables at the measurement height. The blue dots indicate the mean values over the nighttime period at the measurement height. The black solid lines denote the profiles by the numerical model. (For interpretation of the references to colour in this figure legend, the reader is referred to the web version of this article.)

canopy (Baldocchi et al., 1983), and even negative temperature gradient near the ground surface. However, the predicted temperature profiles mismatch tower measurements. The mismatch between modeled and measured temperature is caused by the heat flux configuration such that the full energy balance equation is simplified to an outgoing radiative cooling. The temperature in the canopy was found to be very sensitive to water stress in crops (Jensen et al., 1990) but this is not integrated as a forcing in our model.

The other uncertainties in solving the local scale topographic-canopy- flow arise from the rough topography data, vegetation classification and homogeneous soil respiration rate. The SRTM 90 m digital elevation data is very rough compared to 4 m horizontal grid spacing in our model setting. Many details of the topographic flow cannot be resolved on this 90 m topography resolution. The real vegetation distribution is much more complicated than the three-category classification. The 14.7% of the bare land in the 240 m × 240 m area (Montagnani et al., 2009) is not classified in our model configuration. Improvements are expected with continuous canopy structure retrieved by airborne LiDAR (Marcolla et al., 2014). In addition, the tower measurements we used from ADVEX campaign were collected in July 2005, while the field survey of vegetation classification was done in October 2009. The change in vegetation distribution can contribute to the mismatch between the modeled and measured data. The transfer of $CO_2$ within the canopy relies on $CO_2$ levels and canopy flow. Local $CO_2$ level is determined by turbulent mixing and strength of net $CO_2$ exchange. However, the heterogeneous soil surface $CO_2$ emission (Acosta et al., 2013) due to the heterogeneous vegetation and soil property is not considered in our simulations.

Please cite this article in press as: Xu, X., et al., Numerical study of the interplay between thermo-topographic slope flow and synoptic flow on canopy transport processes. Agric. Forest Meteorol. (2017), http://dx.doi.org/10.1016/j.agrformet.2017.03.004

## 5. Summary and conclusions

We apply a computational fluid dynamics model to investigate nocturnal flow dynamics and associated thermal and $CO_2$ transport under different synoptic forcing in a forested complex terrain at Renon, Italy. In the absence of synoptic-scale forcing, thermal-driven topographic flow dominates, which is characterized by weak (a maximum wind speed of $0.22\,\mathrm{m\,s^{-1}}$) local down-slope northerly winds. The down slope winds blow throughout the vegetation canopy and contribute to rich $CO_2$ accumulation within the canopy in the downwind direction. The modification of local slope winds by synoptic northerlies is limited to above the canopy. However, the northerlies significantly intensify local slope winds. Recirculation is developed in the S-N direction when prevailing northerlies blow down-slope into re-growth forest that has high leaf density in the lower canopy exerting large drag force on canopy flow. The wind direction of local slope winds can be modified by the weaker southerlies all through the canopy and up to triple canopy height; above that the local slope winds disappear. The interactions of local slope wind and southerlies result in reduced up-slope southerlies on the upper slope and dominant down-slope wind on the lower steep slope where the local down-slope winds exceed the southerlies.

Temperature distribution indicated that dense mature and re-growth forest canopies are subject to stronger cooling in the upper canopy. The upper canopy cooling has minor influence on the thermal conditions in the deep canopy because the layer with high foliage density reduces vertical heat transfer, leading to very weak inversions in the deep canopy. In contrast, in the sparse trees in grassland, cooling at the ground surface overwhelms cooling in the canopy, resulting in strong inversions near the ground surface. Radiative cooling is the primary driving force of the within-canopy down-slope winds. The correlation between thermal condition and wind microstructures in the canopy is obvious during northerly wind periods, which is expressed as the cooler recirculation in the S-N direction, and updraft occurring when winds blow from cooler regions to warmer regions in the W-E direction.

The local down-slope winds throughout vegetation canopy contribute to $CO_2$ accumulation within canopy in the downwind direction. During northerly wind periods, recirculation in the S-N direction is characterized by high levels of $CO_2$ up to the top of reversed flow, while $CO_2$ is built up in a very shallow layer in W-E direction where flow subsides from east to west. The updraft motion above the subsided flow does not affect $CO_2$ in the shallow surface layer, as the main $CO_2$ source is the ground surface. Compared with northerly wind and local slope wind periods, there is no extensive $CO_2$ accumulation during southerly wind periods, which is attributed to the cross-slope winds resulting in better mixing. However, a shallow layer with relatively high $CO_2$ concentration is found near the ground surface, which is attributed to the nocturnal air sinking.

Our application of RANS in three-dimensional canopy represents an advance in the modeling of interactions between local thermo-topographic slope flow and large-scale synoptic flow. However, this model shows a weaker representation of large-scale synoptic influences. Downscaling techniques, such as coupled meteorological and RANS models, are necessary to improve the prediction of large scale forcing. In addition, high-resolution and large scale topography, vegetation and $CO_2$ efflux data will help to solve the thermo-topographic slope flows and related ecosystem-atmosphere exchanges.

## Acknowledgements

We are grateful to three anonymous reviewers for their insightful comments and constructive criticisms that have improved our manuscript. This research was supported, in part, under National Science Foundation (NSF) Grant No. ATM-0930015, Grants for computing time from the City University of New York High Performance Computing Center under NSF Grants No. CNS-0958379 and CNS-0855217, and PSC-CUNY Research Awards (Enhanced) No. ENHC-42-64. We thank the group from Forest Services of the Autonomous Province of Bolzano, Italy, for contributing the ADVEX measurement data.

## Appendix A.

The empirical constants $a$ and $b$ in Eq. (7) are determined by the heat flux $Q_h$ at the top of the canopy and $Q_g$ on the ground surface

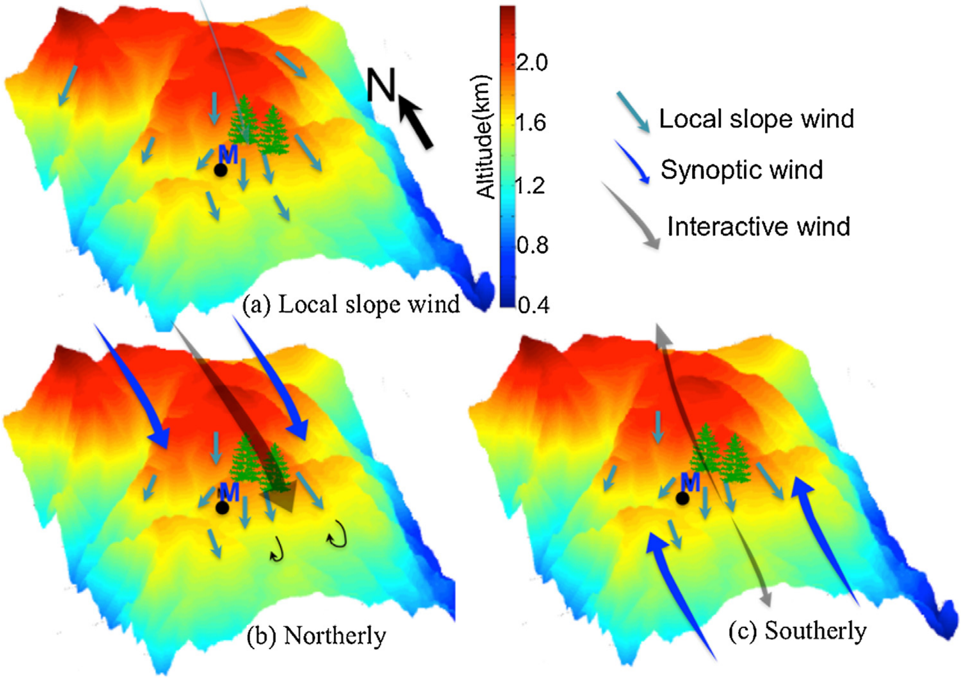

**Fig. A1.** The schematic diagram of the interactions between local slope flow and synoptic winds around Tower M (a 10 km terrain domain) (a) Local slope wind only, (b) Northerly and (c) Southerly.

Please cite this article in press as: Xu, X., et al., Numerical study of the interplay between thermo-topographic slope flow and synoptic flow on canopy transport processes. Agric. Forest Meteorol. (2017), http://dx.doi.org/10.1016/j.agrformet.2017.03.004

**Table A1**
The values of *a* and *b* for each wind-vegetation condition.

| *a*/*b* | Northerly | Southerly | Slope Wind |
|---|---|---|---|
| 1. Sparse forest, Grassland | 112.8/65.3 | −8.9/6.5 | −29.6/19.0 |
| 2. Forest edges, regrowth forest | −51.2/3.7 | −4.1/1.6 | −13.4/2.9 |
| 3. Mature forest | −50.9/3.4 | −4.0/1.6 | −13.3/2.8 |

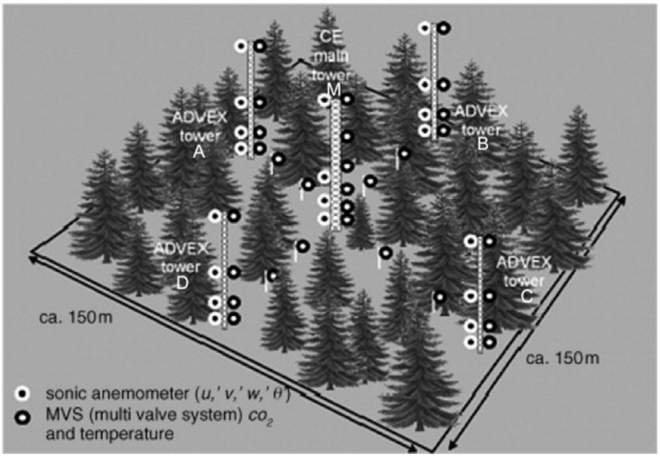

**Fig. A2.** The tower and instruments set-up during ADVEX campaigns. Source: Feigenwinter et al. (2008).

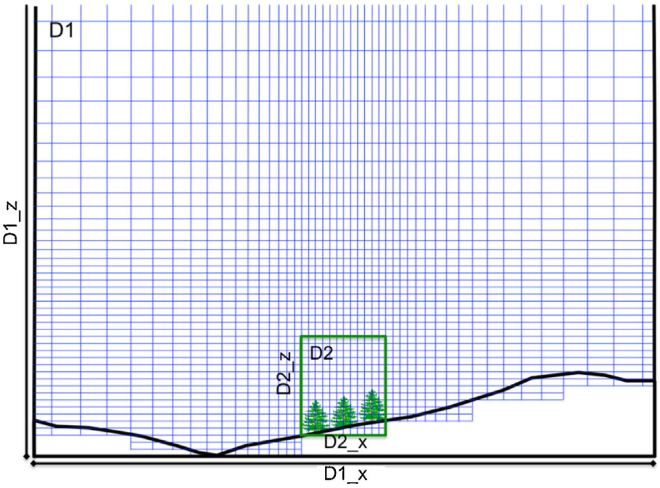

**Fig. A3.** The schematic diagram of the mesh at the intersection of Tower M. D1_x and D1_z are the domain size in the horizontal and vertical for D1. D2_x and D1_z are the domain size in the horizontal and vertical for D2. The mesh setting for our simulation is about 5 times finer in horizontal and 3 times finer in vertical than that shown in the diagram.

for each wind-vegetation condition. The values of *a* and *b* are shown in the Table A1.

## References

Acosta, M., Pavelka, M., Montagnani, L., Kutsch, W., Lindroth, A., Juszczak, R., Janouš, D., 2013. Soil surface $CO_2$ efflux measurements in Norway spruce forests: comparison between four different sites across Europe–from boreal to alpine forest. Agric. For. Meteorol. 192, 295–303.

Araújo, A.C., Kruijt, B., Nobre, A.D., Dolman, A.J., Waterloo, M.J., Moors, E.J., de Souza, J.S., 2008. Nocturnal accumulation of $CO_2$ underneath a tropical forest canopy along a topographical gradient. Ecol. Appl. 18, 1406–1419.

Aubinet, M., Feigenwinter, C., 2010. Direct $CO_2$ advection measurements and the night flux problem. Agric. For. Meteorol. 150, 651–654.

Aubinet, M., Heinesch, B., Yernaux, M., 2003. Horizontal and vertical $CO_2$ advection in a sloping forest. Bound.-Layer Meteorol. 108, 397–417.

Aubinet, M., Feigenwinter, C., Heinesch, B., Bernhofer, C., Canepa, E., Lindroth, A., Montagnani, L., Rebmann, C., Sedlak, P., Van Gorsel, E., 2010. Direct advection measurements do not help to solve the night-time $CO_2$ closure problem: evidence from three different forests. Agric. For. Meteorol. 150, 655–664.

Aubinet, M., 2008. Eddy covariance $CO_2$ flux measurements in nocturnal conditions: an analysis of the problem. Ecol. Appl. 18, 1368–1378.

Baldocchi, D.D., Meyers, T., 1998. On using eco-physiological, micrometeorological and biogeochemical theory to evaluate carbon dioxide, water vapor and trace gas fluxes over vegetation: a perspective. Agric. For. Meteorol. 90, 1–25.

Baldocchi, D.D., Verma, S.B., Rosenberg, N.J., 1983. Microclimate in the soybean canopy. Agric. Meteorol. 28, 321–337.

Belcher, S.E., Finnigan, J.J., Harman, I.N., 2008. Flows through forest canopies in complex terrain. Ecol. Appl. 18, 1436–1453.

Belcher, S.E., Harman, I.N., Finnigan, J.J., 2012. The wind in the willows: flows in forest canopies in complex terrain. Annu. Rev. Fluid Mech. 44, 479–504.

Chen, H., Yi, C., 2012. Optimal control of katabatic flows within canopies. Q. J. R. Meteorol. Soc. 138, 1676–1680.

Dupont, S., Patton, E.G., 2012. Influence of stability and seasonal canopy changes on micrometeorology within and above an orchard canopy: the CHATS experiment. Agric. For. Meteorol. 157, 11–29.

Feigenwinter, C., Bernhofer, C., Vogt, R., 2004. The influence of advection on the short term $CO_2$-budget in and above a forest canopy. Bound.-Layer Meteorol. 113, 201–224.

Feigenwinter, C., Bernhofer, C., Eichelmann, U., Heinesch, B., Hertel, M., Janous, D., Kolle, O., Lagergren, F., Lindroth, A., Minerbi, S., Moderow, U., Mölder, M., Montagnani, L., Queck, R., Rebmann, C., Vestin, P., Yernaux, M., Zeri, M., Ziegler, W., Aubinet, M., 2008. Comparison of horizontal and vertical advective $CO_2$ fluxes at three forest sites. Agric. For. Meteorol. 148, 12–24.

Feigenwinter, C., Montagnani, L., Aubinet, M., 2010a. Plot-scale vertical and horizontal transport of $CO_2$ modified by a persistent slope wind system in and above an alpine forest. Agric. For. Meteorol. 150, 665–673.

Feigenwinter, C., Mölder, M., Lindroth, A., Aubinet, M., 2010b. Spatiotemporal evolution of $CO_2$ concentration, temperature, and wind field during stable nights at the Norunda forest site. Agric. For. Meteorol. 150, 692–701.

Finnigan, J.J., 2008. An introduction to flux measurements in difficult conditions. Ecol. Appl. 18, 1340–1350.

Flesch, T.K., Prueger, J.H., Hatfield, J.L., 2002. Turbulent Schmidt number from a tracer experiment. Agric. For. Meteorol. 111, 299–307.

Goulden, M.L., Miller, S.D., da Rocha, H.R., 2006. Nocturnal cold air drainage and pooling in a tropical forest. J. Geohys. Res. D 111 (D8), http://dx.doi.org/10.1029/2005jd006037.

Gross, G., 1993. Numerical Simulation of Canopy Flows. In: Douglas, J., Marcus, M. (Eds.). Springer, Berlin, p. 167.

Haiden, T., Whiteman, C.D., 2005. Katabatic flow mechanisms on a low-angle slope. J. Appl. Meteorol. 44, 113–126.

Hoener, S.F., 1965. Fluid Dynamic Drag: Practical Information on Aerodynamic Drag and Hydrodynamic Resistence, Midland Park, N.J.

Jacobs, A.F.G., Van Boxel, J.H., El-Kilani, M.M., 1994. Nighttime free convection characteristics within a plant canopy. Bound.-Layer Meteorol. 71, 375–391.

Janssens, I.A., Lankreijer, H., Matteucci, G., Kowalski, A.S., Buchmann, N., Epron, D., Pilegaard, K., Kutsch, W., Longdoz, B., Grünwald, T., Montagnani, L., Dore, S., Rebmann, C., Moors, E.J., Grelle, A., Ü, Rannik, Morgenstern, K., Oltchev, S., Clement, R., Gudmundsson, J., Minerbi, S., Berbigier, P., Ibrom, A., Moncrieff, J., Aubinet, M., Bernhofer, C., Jensen, N.O., Vesala, T., Granier, A., Schulze, E.-D., Lindroth, A., Dolman, A.J., Jarvis, P.G., Ceulemans, R., Valentini, R., 2001. Productivity overshadows temperature in determining soil and ecosystem respiration across European forests. Glob. Change Biol. 7, 269–278.

Jarvis, A., Reuter, H.I., Nelson, A., Guevara, E., 2008. Hole-filled SRTM for the Globe Version 4 Available from the CGIAR-CSI SRTM 90 M Database. http://srtm.csi.cgiar.org.

Jensen, H.E., Svendsen, H., Jensen, S.E., Mogensen, V.O., 1990. Canopy-air temperature of crops grown under different irrigation regimes in a temperate humid climate. Irrig. Sci. 11, 181–188.

Kim, H.G., Patel, V.C., 2000. Test of turbulence models for wind flow over terrain with separation and recirculation. Bound.-Layer Meteorol. 94, 5–21.

Law, B.E., Kelliher, F.M., Baldocchi, D.D., Anthoni, P.M., Irvine, J., Moore, D., Van Tuyl, S., 2001. Spatial and temporal variation in respiration in a young ponderosa pine forest during a summer drought. Agric. For. Meteorol. 110, 27–43.

Mahrt, L., Lee, X., Black, A., Neumann, H., Staebler, R.M., 2000. Nocturnal mixing in a forest subcanopy. Agric. For. Meteorol. 101, 67–78.

Marcolla, B., Cobbe, I., Minerbi, S., Montagnani, L., Cescatti, A., 2014. Methods and uncertainties in the experimental assessment of horizontal advection. Agric. For. Meteorol. 198–199, 62–71.

Massman, W.J., Lee, X., 2002. Eddy covariance flux corrections and uncertainties in long term studies of carbon and energy exchanges. Agric. For. Meteorol. 113, 121–144.

Montagnani, L., Manca, G., Canepa, E., Georgieva, E., Acosta, M., Feigenwinter, C., Janous, D., Kerschbaumer, G., Lindroth, A., Minach, L., Minerbi, S., Mölder, M., Pavaelka, M., Seufert, G., Zeri, M., Ziegler, W., 2009. A new mass conservation approach to the study of $CO_2$ advection in an alpine forest. J. Geophys. Res. 114, D07306, http://dx.doi.org/10.1029/2008JD010650.

Montagnani, L., Manca, G., Canepa, E., Georgieva, E., 2010. Assessing the method-specific differences in quantification of $CO_2$ advection at three forest sites during the ADVEX campaign. Agric. For. Meteorol. 150, 702–711, http://dx.doi.org/10.1016/j.agrformet.2010.01.013.

Ohkubo, S., Kosugi, Y., Takanashi, S., Mitani, T., Tani, M., 2007. Comparison of the eddy covariance and automated closed chamber methods for evaluating

Please cite this article in press as: Xu, X., et al., Numerical study of the interplay between thermo-topographic slope flow and synoptic flow on canopy transport processes. Agric. Forest Meteorol. (2017), http://dx.doi.org/10.1016/j.agrformet.2017.03.004

nocturnal $CO_2$ exchange in a Japanese cypress of forest. Agric. For. Meteorol. 142, 50–65.

Pierce, L.L., Running, S.W., 1988. Rapid estimation of coniferous forest leaf area index using a portable integrating radiometer. Ecology 69, 1762–1767.

Reiners, W.A., Anderson, R.O., 1968. $CO_2$ concentrations in forests along a topographic gradient. Am. Midl. Nat. 80, 111–117.

Rolland, C., 2002. Spatial and seasonal variations of air temperature lapse rates in Alpine regions. J. Clim. 16, 1032–1046.

Santana, R.A.S., Dias-Junior, C.Q., Val, R.S.D., Tota, J., Fitzjarrald, D.R., 2017. Observing and Modeling the Vertical Wind Profile at Multiple Sites in and Above the Amazon Rain Forest Canopy, Advances in Meteorology., http://dx.doi.org/10.1155/2017/5436157, Article ID 5436157, 8 pages.

Sedlák, P., Aubinet, M., Heinesch, B., Janouš, D., Pavelka, M., Potužníková, K., Yernaux, M., 2010. Night-time airflow in a forest canopy near a mountain crest. Agric. For. Meteorol. 150, 736–744.

Shaw, R.H., den Hartog, G., Neumann, H.H., 1988. Influence of foliar density and thermal-stability on profiles of Reynolds stress and turbulence intensity in a deciduous forest. Bound.-Layer Meteorol. 45, 391–409.

Sun, J., Burns, S.P., Delany, A.C., Oncley, S.P., Turnipseed, A.A., Stephens, B.B., Lenschow, D.H., LeMone, M.A., Monson, R.K., Anderson, D.E., 2007. $CO_2$ transport over complex terrain. Agric. For. Meteorol. 145, 1–21.

Tóta, J., Fitzjarrald, D.R., da Silva Dias, M.A.F., 2012. Amazon rainforest exchange of carbon and subcanopy air flow: manaus LBA site-a complex terrain condition. Sci. World J. 2012, 165067, http://dx.doi.org/10.1100/2012/165067.

Turnipseed, A.A., Anderson, D.E., Blanken, P.D., Baugh, W.M., Monson, R.K., 2003. Airflows and turbulent flux measurements in mountainous terrain. Part 1. Canopy and local effects. Agric. For. Meteorol. 119, 1–21.

Urban, O., Janouš, D., Acosta, M., Czerný, R., Marková, I., Navrtil, M., Pavelka, M., Pokorný, R., Šprtov, M., Zhang, R., Špunda, V., Grace, J., Marek, M., 2007. Ecophysiological controls over the net ecosystem exchange of mountain spruce stand. Comparison of the response in direct vs. diffuse solar radiation. Glob. Change Biol. 13, 157–168.

Van t'Hoff, J.H., 1884. Études De Dynamique Chimique. F. Muller & Co., Amsterdam.

Vickers, D., Mahrt, L., 2006. Contrasting mean vertical motion from tilt correction methods and mass continuity. Agric. For. Meteorol. 138, 93–103.

Wilson, J.D., 1986. On the choice of a windbreak porosity profile. Bound.-Layer Meteorol. 38, 37–49.

Xu, X., Yi, C., 2013. The influence of geometry on recirculation and $CO_2$ transport over forested hills. Meteorol. Atmos. Phys. 119, 187–196.

Xu, X., Yi, C., Kutter, E., 2015. Stably stratified canopy flow in complex terrain. Atmos. Chem. Phys. 15, 7457–7470.

Yakhot, V., Orszag, S.A., 1986. Renormalization group analysis of turbulence: basic theory. J. Sci. Comput. 1, 3–61.

Yakhot, V., Smith, L.M., 1992. The renormalization group, the e-expansionand derivation of turbulence models. J. Sci. Comput. 7, 35–61.

Yakhot, V., Orszag, S.A., Thangam, S., Gatski, T.B., Speziale, C.G., 1992. Development of turbulence models for shear flows by a double expansion technique. Phys. Fluids A 4, 1510–1520.

Yamazaki, H., Satomura, T., 2010. Nonhydrostatic atmospheric modeling usng a combined Cartesian grid. Mon. Weather Rev. 138, 3932–3945.

Yi, C., Davis, K.J., Bakwin, P.S., Berger, B.W., Marr, L.C., 2000. Influence of advection on measurements of the net ecosystem–atmosphere exchange of CO2 from a very tall tower. J. Geophys. Res. 105 (D8), 9991–9999.

Yi, C., Monson, R.K., Zhai, Z., Anderson, D.E., Lamb, B., Allwine, G., Turnipseed, A.A., Burns, S.P., 2005. Modeling and measuring the nocturnal drainage flow in a high-elevation, subalpine forest with complex terrain. J. Geophys. Res. 110, D22303, http://dx.doi.org/10.1029/2005JD006282.

Yi, C., Anderson, D.E., Turnipseed, A.A., Burns, S.P., Sparks, J.P., Stannard, D.I., Monson, R.K., 2008. The contribution of advective fluxes to net ecosystem exchange in a high-elevation, subalpine forest. Ecol. Appl. 18 (6), 1379–1390.

Yi, C., 2008. Momentum transfer within canopies. J. Appl. Meteorol. Climatol. 47, 262–275, http://dx.doi.org/10.1175/2007JAMC1667.1.

Please cite this article in press as: Xu, X., et al., Numerical study of the interplay between thermo-topographic slope flow and synoptic flow on canopy transport processes. Agric. Forest Meteorol. (2017), http://dx.doi.org/10.1016/j.agrformet.2017.03.004